Review of Scientific Instruments

Development of a density-tapered capillary gas cell for laser wakefield acceleration

Cite as: Rev. Sci. Instrum. **92**, 023511 (2021); https://doi.org/10.1063/5.0009632
Submitted: 02 April 2020 . Accepted: 27 January 2021 . Published Online: 18 February 2021

J. Kim, V. L. J. Phung, K. Roh, M. Kim, K. Kang, and H. Suk

Review of Scientific Instruments ARTICLE scitation.org/journal/rsi

Development of a density-tapered capillary gas cell for laser wakefield acceleration

Cite as: Rev. Sci. Instrum. 92, 023511 (2021); doi: 10.1063/5.0009632
Submitted: 2 April 2020 • Accepted: 27 January 2021 •
Published Online: 18 February 2021

J. Kim,[1] V. L. J. Phung,[1] K. Roh,[1] M. Kim,[2] K. Kang,[1] and H. Suk[1,a)]

AFFILIATIONS

[1] Department of Physics and Photon Science, Gwangju Institute of Science and Technology, Gwangju 61005, South Korea
[2] PAL-XFEL Beamline Division, Pohang Accelerator Laboratory, Pohang 37673, South Korea

[a)] **Author to whom correspondence should be addressed:** hysuk@gist.ac.kr

ABSTRACT

A capillary gas cell for laser wakefield acceleration was developed with the aid of three-dimensional computational fluid dynamics simulations. The gas cell was specially designed to provide upward density tapering in the longitudinal direction, which is expected to suppress the dephasing problem in laser wakefield acceleration by keeping the accelerated electrons in the acceleration phase of the wake wave. The density-tapered capillary gas cell was fabricated by sapphire plates, and its performance characteristics were tested. The capillary gas cell was filled with a few hundred millibars of hydrogen gas, and a Ti:sapphire laser pulse with a peak power of 3.8 TW and a pulse duration of 40 fs (full width at half maximum) was sent through the capillary hole, which has a length of 7 mm and a square cross section of 350 × 350 μm^2. The laser-produced hydrogen plasma in the capillary hole was then diagnosed two-dimensionally by using a transverse Mach–Zehnder interferometer. The capillary gas cell was found to provide an upward plasma density tapering in the range of 10^{18} cm^{-3}–10^{19} cm^{-3}, which has a potential to enhance the electron beam energy in laser wakefield acceleration experiments.

I. INTRODUCTION

In 1979, Tajima and Dawson[1] proposed a novel particle acceleration scheme based on laser–plasma interactions that can provide an extremely high acceleration gradient of ~100 GV/m. This plasma-based acceleration scheme with such a high acceleration gradient may lead to the development of compact high-energy particle accelerators and new radiation sources.[2–4] In this kind of research, a plasma source is one of the most important parts. So far, several different types have been developed, including a gas jet,[5–7] a discharged capillary,[8–11] and a gas cell.[12,13] To generate stable electron beams from the laser wakefield acceleration (LWFA), the plasma source must provide a stable plasma density.[8,14,15] A stable plasma density can be achieved in a gas cell when a high-power laser pulse propagates in the gas cell,[7,16] making it a good plasma source.

Another important issue in LWFA is how to increase the electron energy for a given laser power. The three main factors for energy saturation are known, which include the diffraction of a focused laser pulse, laser energy depletion in the plasma, and the dephasing problem. The diffraction problem can be solved by a plasma waveguide[18–20] with a parabolic density profile in the transverse direction or by the relativistic self-focusing of the intense laser pulse in the plasma. The energy depletion problem can be avoided by staging of the plasma source and laser.[21,22] The dephasing problem, which is caused by the velocity difference between the accelerated electron beam and the wake wave in the plasma, can be solved by upward density tapering along the longitudinal direction.[23,24] Density tapering allows the injected electrons to be accelerated to higher energies because in the upward density profile, the electron beam can stay continuously in the acceleration phase.[23,24] Further acceleration for even higher energies may be achieved by multi-staged laser-plasma accelerators.[21,22,25]

To avoid the dephasing problem, we developed a special capillary gas cell that can provide a stable plasma density and upward density tapering along the longitudinal direction. Furthermore, we implemented a three-dimensional (3D) structure of a capillary system using 3D computational fluid dynamics (CFD) simulations. We tested the performance characteristics of the capillary gas cell with a femtosecond-laser-based Mach–Zehnder interferometer, leading to complete two-dimensional (2D) plasma density profiles. Our results show that the capillary gas cell can provide a stable plasma electron

density with a density tapering in the range of $N_e = 10^{18}$ cm^{-3}–10^{19} cm^{-3}, which may enhance the electron beam energy in LWFA.[23,24] In this paper, we describe the details of the developed capillary gas cell.

II. CAPILLARY GAS CELL DEVELOPMENT

A. 3D CFD simulations

To design the capillary gas cell, we performed 3D CFD simulations using the student version of the commercial code ANSYS FLUENT.[26] While the CFD simulation cannot fully reproduce all of the experimental conditions, it may give a rough tendency and idea for design in our case.

The 3D structure for the simulations consists of a 7-mm-long capillary hole with a square cross section of 350 × 350 μm^2 and two gas feedlines, as shown in Fig. 1(a). Hydrogen gas is injected into the feedline 1 and feedline 2 with input pressures of 200 mbar and 600 mbar, respectively, to achieve a density gradient along the longitudinal direction. The injected hydrogen gas flows into the capillary hole and is ejected from both ends of the capillary. The gas dynamics in the capillary gas cell was studied by CFD simulations in which the Navier–Stokes equation is numerically solved with an implicit density-based solver for the capillary gas cell can be realized by varying the input gas pressures at the feedlines, and Fig. 1(b) shows the gas density distributions in the capillary gas cell for various situations. The gas feedlines [gray shading in Fig. 1(b)] are located 1 mm away from both edges of the 7-mm-long capillary hole. The CFD simulations imply that the longitudinal density profile can be controlled by adjusting the input pressure and feedline width. The result shows that the density gradient in the capillary gas cell can be controlled by adjusting the pressures and further enhancement of tapering is achievable using different feedline widths.

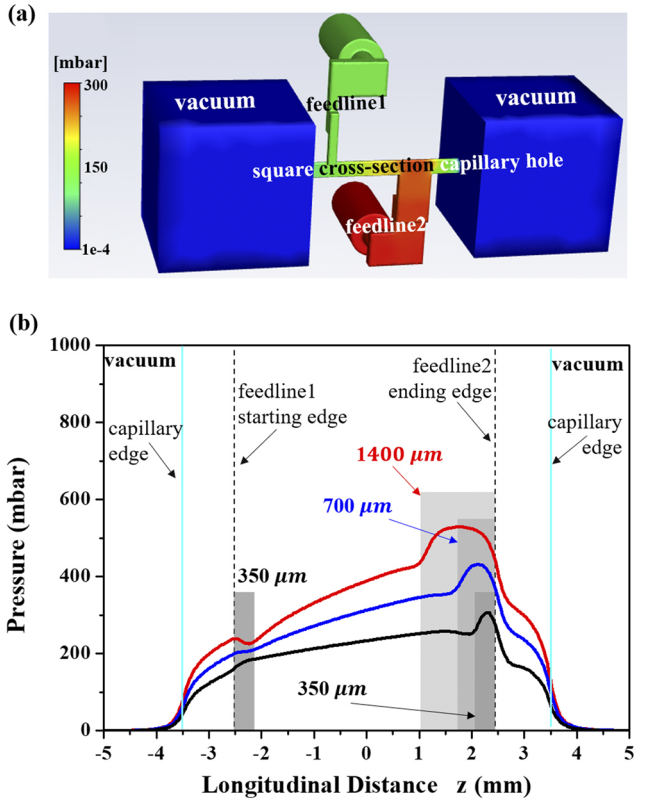

FIG. 1. 3D CFD simulation results for a capillary gas cell with a capillary hole length of 7 mm and a square cross-sectional dimension of 350 × 350 μm^2. (a) A typical 3D CFD simulation result for a hydrogen gas pressure (density) distribution in a capillary with two gas feedlines; one with a width of 350 μm and the other with a width of 1400 μm. (b) Longitudinal gas pressure (density) distributions for different widths of the second feedline (350 μm, 700 μm, and 1400 μm) and the first feedline with a fixed width of 350 μm. The first feedline was at 200 mbar, and the second was at 600 mbar.

B. Fabrication of the capillary gas cell

Based on the CFD simulation results, we designed and built a capillary gas cell using sapphire plates. Figure 2(a) shows the assembled capillary gas cell system with its housing, which is small enough to be held in one hand. The sapphire plates were machined by a local company (COMA Technology Co.[27]) according to our design. All machined sapphire plates were polished by an Oscar type polishing machine, and the machining tolerance was kept within ±10 μm.

Figures 2(b) and 2(c) show magnified pictures of the side and front views, respectively, of the assembled capillary. A square cross-sectional capillary hole was formed by placing two thin (350 μm) sapphire plates between two thick (2 mm) sapphire plates, as shown in Figs. 2(c) and 2(d); the thick plates were tied tightly together to avoid gas leakage. Figure 2(e) shows a detailed view of the machined feedline and the through-hole in the thick sapphire plate. Since all of the sapphire plates were polished, they are transparent to the laser beam, allowing laser beam transmission for 2D density mapping using the laser interferometer. Two high-speed solenoid valves (Parker Hannifin, model 009-0181-900) with response times of less than 2 ms were used for the gas injection system, and the gas was injected via the through-hole in one of the thick sapphire plates.

III. EXPERIMENTAL SETUP

To investigate the performance characteristics of the capillary gas cell, we conducted experiments in our laboratory. The experimental setup is shown in Fig. 3. For the characterization experiments, nitrogen gas was used for the neutral gas density measurement, and hydrogen gas was used for the laser-induced plasma density measurement in the capillary. For our laser wakefield acceleration experiments, hydrogen gas will be used in the capillary. Ideally, all gas and plasma density measurements should be done using hydrogen gas, but the phase shift by hydrogen gas along a distance of a few hundred micrometers is too small to analyze. Instead of hydrogen, therefore, we used nitrogen gas that has a significantly higher refractive index than hydrogen. Using CFD simulations, we confirmed that nitrogen and hydrogen show similar density distributions in the capillary gas cell for the same input pressures at the feedlines, as shown in Fig. 4.

For the laser-induced plasma density measurement, we used the 20 TW/40 fs Ti:sapphire laser system[28] in our laboratory at the Gwangju Institute of Science and Technology (GIST). Specifically, only 200 mJ of the pulse energy was used for the laser-induced plasma diagnostics. This Ti:sapphire laser system had a

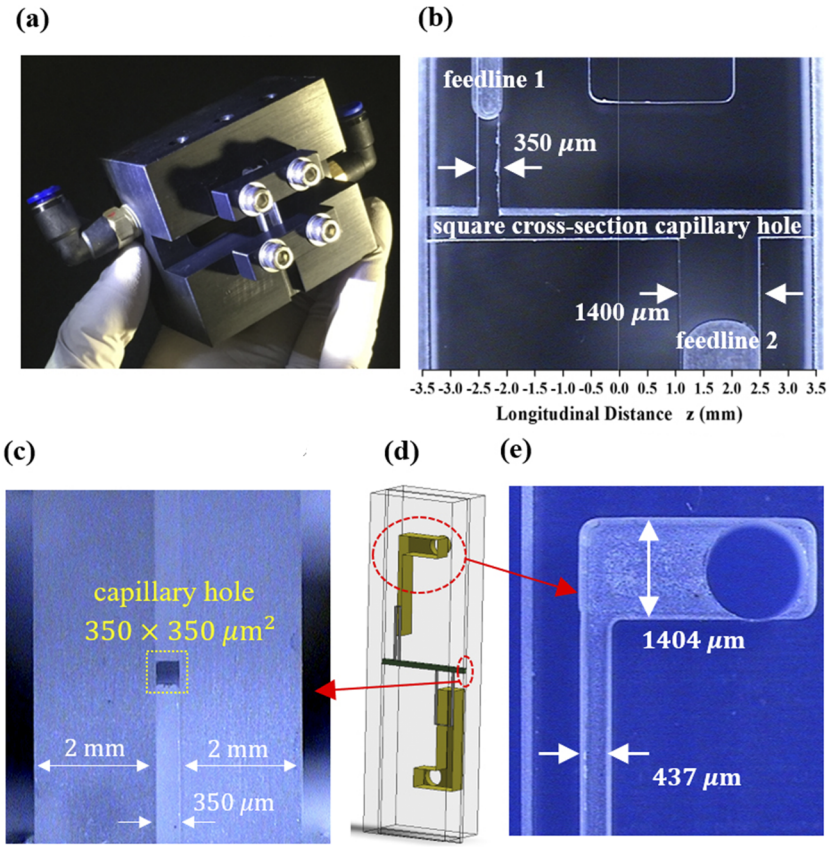

FIG. 2. Detailed pictures of the capillary gas cell. (a) Assembled capillary gas cell system with its housing. Magnified images of the side (b) and front (c) views of the assembled capillary. (d) The 3D modeling structure of the assembled capillary. (e) Detailed view of the through-hole and the machined feedline in the thick sapphire plate.

center wavelength of 805 nm with a spectral bandwidth of 37 nm. The pulse duration (τ_L) was about 40 fs full width at half maximum (FWHM), which was measured by the frequency-resolved optical gating (FROG) method (Fastlite, GRENOUILLE). The high-power laser beam was divided into two beams before the off-axis parabolic (OAP) mirror, as shown in Fig. 3. One beam was the reflected driving laser pulse for plasma generation in the capillary hole, and the other beam was the transmitted probe laser pulse, which had only 0.3% (0.6 mJ/pulse) of the driving pulse energy for the transverse interferometer.

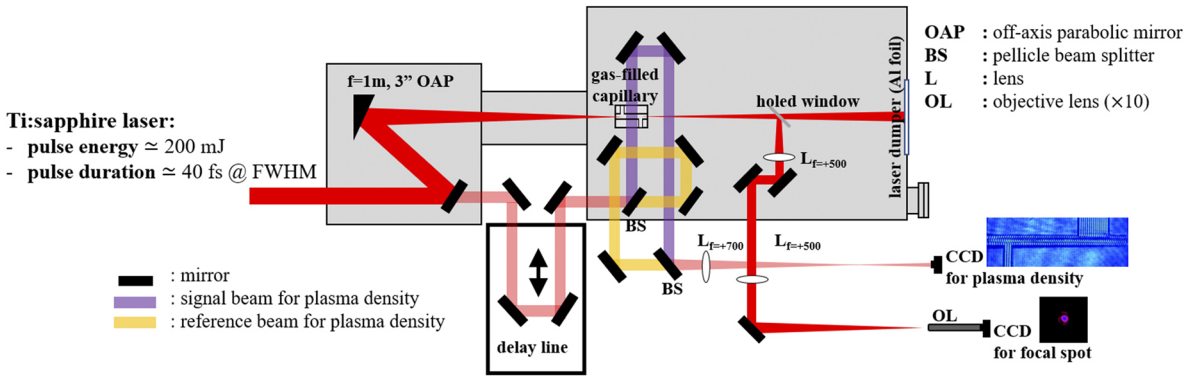

FIG. 3. Experimental setup for the capillary plasma density measurement using a Mach–Zehnder interferometer. The main driving laser pulse to the capillary hole has an energy of 200 mJ/pulse and a pulse duration of around 40 fs. A small portion of the main laser pulse passing through the mirror before the OAP is used for the Mach–Zehnder interferometer.

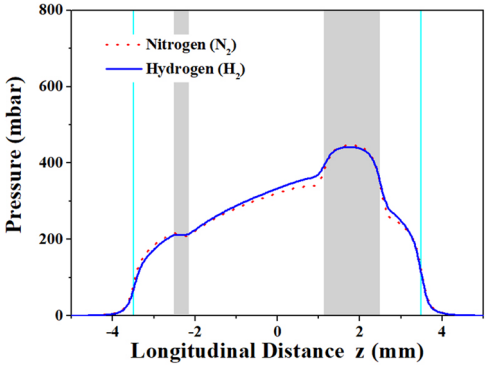

FIG. 4. Comparison between nitrogen and hydrogen. At a given pressure, the CFD simulation results show similar density distributions in the capillary gas cell for the two gases.

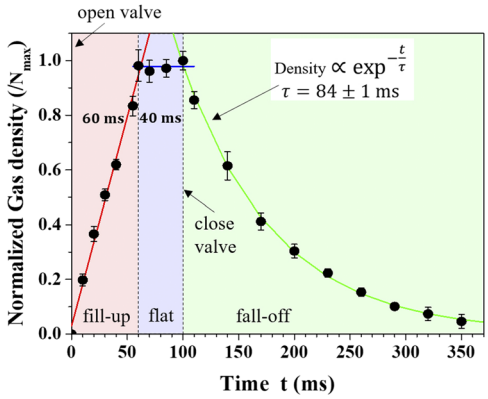

FIG. 5. Gas density temporal evolution in the capillary gas cell. The valve was opened for 100 ms to inject the nitrogen gas into the capillary gas cell. The capillary gas cell was full after 60 ms and retained the maximum density for 40 ms before decaying exponentially with a decay time constant of 85.4 ms.

The probe pulse had the same center wavelength and spectral bandwidth as those of the driving pulse, although the pulse duration was slightly longer (43 fs) due to transmission through several optical elements. The driving laser pulse was focused onto a spot diameter of 30 μm (FWHM), which corresponds to the peak intensity of $I_0 \simeq 4 \times 10^{17}$ W/cm^2. The focusing position was adjusted around the feedline 1 of the capillary gas cell. This focused laser intensity is strong enough to ionize the hydrogen atoms completely because it is much higher than the hydrogen ionization intensity of 1.4×10^{14} W/cm^2.[29] The focused laser beam has the Rayleigh length of around 2.5 mm and has a waist of 24 μm at $1/e^2$. The plasma density profiles in the capillary hole were measured by the Mach–Zehnder interferometry using the transmitted probe beam. As shown in Fig. 3, the probe laser pulse was time-delayed by the delay line, and then, it was sent to the Mach–Zehnder interferometer for plasma diagnostics. In the interferometer, the probe laser beam was divided by the pellicle beam splitter (BS) into two beam lines. One beam passes through the laser-induced plasma transversely (purple line in Fig. 3), and the other beam is used as a reference (yellow line in Fig. 3). Merging the two laser pulses results in an interferogram that includes the plasma density information by the phase shift. The probe laser beam size in the interferometer was large enough to cover the entire capillary. For the neutral gas density measurement, a nanosecond frequency-doubled Nd:YAG laser was used as the interferometer probe beam, and the beam line was shared with the signal beam line for the plasma density measurement. For the performance characterization experiment, we used a capillary gas cell with a length of 7 mm and feedline widths of 350 μm and 1400 μm. Nitrogen or hydrogen gas was injected into the feedline 1 and feedline 2 to generate longitudinal density profiles.

IV. RESULTS

Before performing the laser-induced plasma density measurement, the temporal evolution of the gas density in the capillary was measured using the nanosecond interferometer as shown in Fig. 5, where the valve was kept open for 100 ms. The gas density in the capillary gas cell increases almost linearly after opening the valve, and the gas cell is completely filled up after 60 ms. This rather long filling time is due to the 20-cm-long gas tube between the pulsed solenoid valve and the gas feedline of the capillary. If we consider only the capillary itself, it may take a few hundred microseconds. The peak density remains for 40 ms, and then, it decays exponentially with a decay time constant of $\tau = 85.4$ ms. The fact that the peak gas density remains constant for 40 ms means that we can reduce the valve opening time significantly for the laser wakefield acceleration experiment, always considering the filling time of the tube between the valve and capillary.

We also used a high-power laser pulse to measure the gas density just outside the capillary, as it may play an important role in LWFA. Figure 6 shows the gas density distribution near the capillary entrance. The gas density at the entrance is about 30% of the density inside, and it decreases to about 10% of the inside density at a distance of 0.6 mm from the capillary entrance.

For the plasma density measurement, the 200-mJ driving laser pulse was sent through the capillary hole filled with hydrogen gas, and the transverse Mach–Zehnder interferometer was used for plasma diagnostics. Figures 7(a) and 7(b) show the interferograms without and with the driving laser pulse, respectively. Figure 7(b) was obtained 24 ps after the driving laser pulse entered the capillary entrance, that is, it is just after the driving laser pulse exited the 7-mm-long capillary gas cell. It should be noted here that the timing difference between the driving laser pulse and the probe laser pulse was adjusted very carefully by the delay line. As shown in Fig. 7(b), the focused driving laser pulse propagates from left to right as indicated by the green arrow, producing clear phase changes along the axis of the capillary gas cell. This result implies that the driving laser pulse generated a laser-induced plasma channel by ionization of the hydrogen atoms in the capillary cell, which is expected given that the focused intensity of the driving laser pulse is much higher than the ionization threshold of hydrogen atoms. Hence, analysis of the interferogram in Fig. 7(b) can provide the plasma density profile along the capillary hole. To analyze the interferograms, we subtracted the reference interferogram (without the plasma) from the signal interferogram (with the laser-induced plasma). The Abel transform technique was employed to obtain the absolute density. The measured phase shift $\varphi(y)$and the electron density have

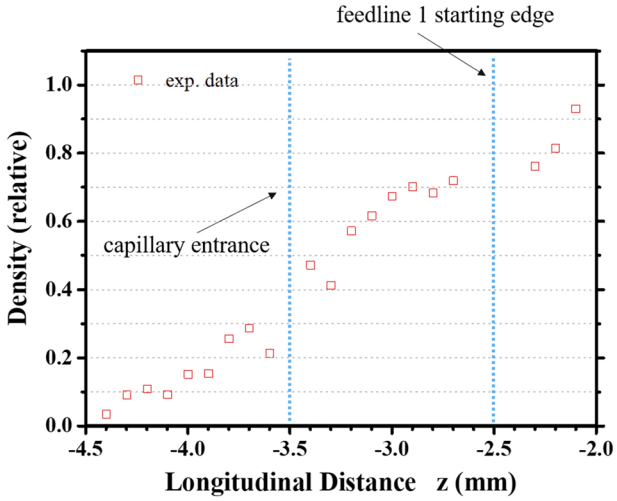

FIG. 6. Gas density distribution near the capillary entrance. The squares show the experimental results. The capillary entrance edge and the feedline 1 starting edge are indicated by the vertical blue lines at $z = -3.5$ mm and $z = -2.5$ mm, respectively.

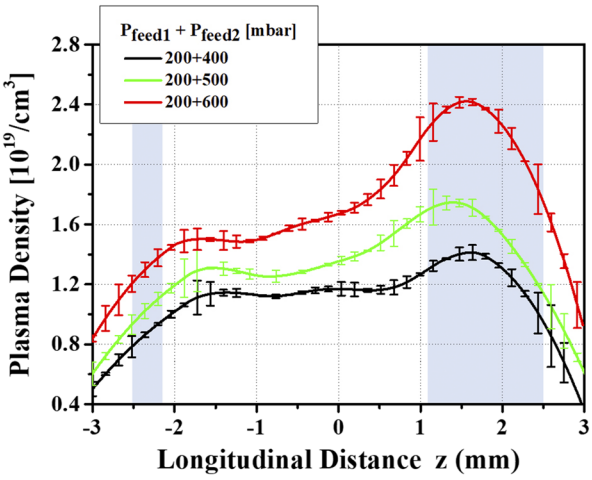

FIG. 8. Longitudinal plasma electron density profiles in the capillary gas cell. The hydrogen gas was injected into the feedline 1 at 200 mbar, while the feedline 2 hydrogen gas pressure was set to 400 mbar, 500 mbar, or 600 mbar. Note that the feedline 1 has a width of 350 μm, while the feedline 2 has a width of 1400 μm.

the following relation:[30]

$$\varphi(y) = -\left(\frac{2\pi}{\lambda N_{cr}}\right)\int_y^{r_p} \frac{N_e(r)}{(r^2 - y^2)^{1/2}} rdr,$$

where N_{cr} is the critical plasma density and is given by $N_{cr} = 4\pi^2 c^2 m_e \varepsilon_0 / e^2 \lambda^2$. Here, λ is the laser wavelength, r_p is the plasma radius, r is the radial distance from the axis (it has the relation of $r^2 = x^2 + y^2$ in the xy plane), c is the speed of light in vacuum, ε_0 is the electric permittivity of free space, and m_e and e are the electron mass and charge, respectively.

The electron density can be calculated using the inverse Abel transform, which is given by[31]

$$N_e(r) = \left(\frac{\lambda N_{cr}}{\pi^2}\right)\int_r^{r_p} \frac{\partial\varphi(y)}{\partial y} \frac{1}{(y^2 - r^2)^{1/2}} dy.$$

In this way, we obtained the longitudinal plasma density profile by using the transverse Mach–Zehnder interferometer. Figure 7(c) shows some examples of the plasma density profiles at different longitudinal positions in the capillary gas cell.

In the experiment, the input gas pressure for the feedline 1 (P_{feed1}) was 200 mbar for all cases, while the pressure for the feedline 2 (P_{feed2}) was initially 400 mbar ($2 \times P_{feed1}$), but then was increased to 500 mbar ($2.5 \times P_{feed1}$), and finally to 600 mbar ($3.0 \times P_{feed1}$). Figure 8 clearly shows that the pressure ratio can be used to control the longitudinal plasma density profile and its gradient in the capillary gas cell. It should be noted that Fig. 8 does not show the plasma density at the capillary edges; this is mainly due to the diffraction of the probe laser beam by the edge of the capillary, which had an unpolished surface, meaning that the interferogram near the capillary edges could not be analyzed. In addition, the plasma density outside the capillary hole is not shown here, as the femtosecond laser

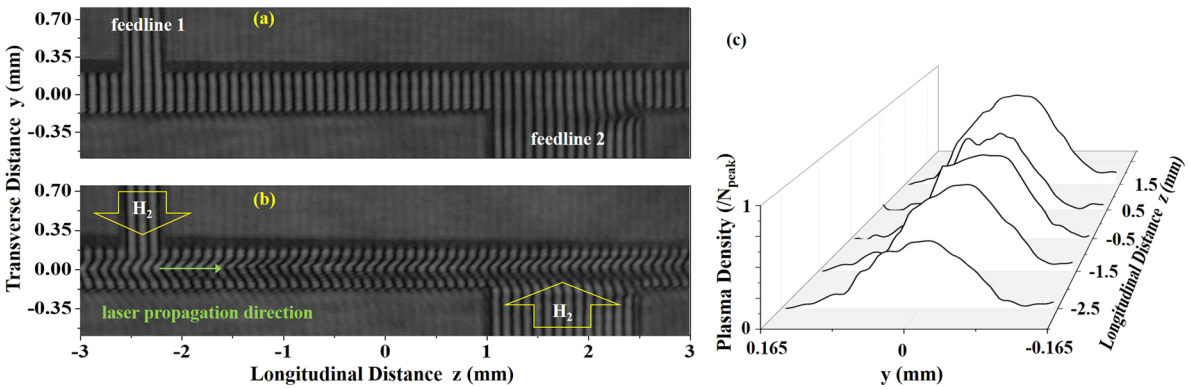

FIG. 7. (a) Interferogram without plasma, (b) interferogram with the laser-induced plasma, and (c) density profiles at different longitudinal positions in the capillary hole. Figures 5(b) and 5(c) show that the driving laser pulse propagates through the capillary hole without a significant beam size change.

interferometer has a limited coherence length.[32] In other words, the optical path difference of the probe beam inside and outside the capillary is calculated to be about 260 μm (considering the refractive index of sapphire) for the laser wavelength of 800 nm, and this is larger than the coherence length, which is in the range of 10 μm–100 μm for a laser pulse of tens of femtosecond duration. Hence, the interferogram cannot simultaneously show a clear image of inside and outside of the capillary.

From the presented interferometric experimental data, it can be seen that there is a self-focusing effect of the high-power driving laser pulse (see Fig. 7). The self-focusing effect requires the peak power of the driving pulse to be higher than the critical power in the plasma, which is given by P_{crit} (GW) $\simeq 17.4 \times (\omega_0/\omega_p)^2$ in practical units,[33] where ω_0 is the angular frequency of the driving laser pulse, and ω_p is the plasma frequency given by $\omega_p = (N_e e^2/m_e \varepsilon_0)^{1/2}$. Based on the induced plasma density at the focal point (around the feedline 1), the critical power is estimated to be $P_{crit} \simeq 3.6$ TW and decreases to less than 1 TW in the high-density region around the feedline 2. The peak power of the driving laser pulse in this experiment is higher than the critical self-focusing power. In the case of a short laser pulse, the self-focusing threshold can be defined by the effective plasma frequency and the duration of the driving pulse[34] as $\omega_p\left(1 + a_0^2/2\right)^{\{-1/4\}}\tau_L \geq 4.6$, where a_0 is the normalized laser amplitude. In our experiment, $\omega_p\left(1 + a_0^2/2\right)^{\{-1/4\}}\tau_L$ was 7, satisfying the self-focusing requirement for a short laser pulse. To confirm the self-focusing effect, we performed PIC simulations using the 2D EPOCH code,[35] which includes the laser-induced ionization process. For the simulations, we used the experimental parameters for the laser beam and hydrogen gas (density and density profile) in the capillary gas cell. Figure 9 shows the simulation results for the evolution of the peak laser field amplitude when the laser pulse propagates in the hydrogen-filled capillary. For the results shown in Fig. 9, the measured plasma density profile for the case where P_{feed2} = 600 mbar (see Fig. 8) was used for the hydrogen gas density.

Figure 9 shows the PIC simulation results obtained for two different laser intensity regimes: (i) a high-intensity laser pulse with $I_0 = 4 \times 10^{17}$ W/cm^2 (fully ionized case) and (ii) a low-intensity laser pulse with $I_0 = 2.5 \times 10^{14}$ W/cm^2 (partially ionized case). In Fig. 9, the dotted blue line shows the hydrogen gas density distribution, and the solid red line indicates the peak field evolution of the driving laser. In the simulation, the laser beam propagated from left to right and interacted with the hydrogen gas. The high-intensity laser pulse produced a fully ionized plasma,[29] and could be self-focused in a high-density plasma regime, as shown in Figs. 9(c) and 9(d). However, it was not self-focused in a low density plasma [see Figs. 9(a) and 9(b)], in which the laser pulse did not satisfy the self-focusing criterion. The low-intensity laser pulse does not satisfy the self-focusing condition, either, so in this low-intensity case, the ionization-induced diffraction effect is dominant, as shown in

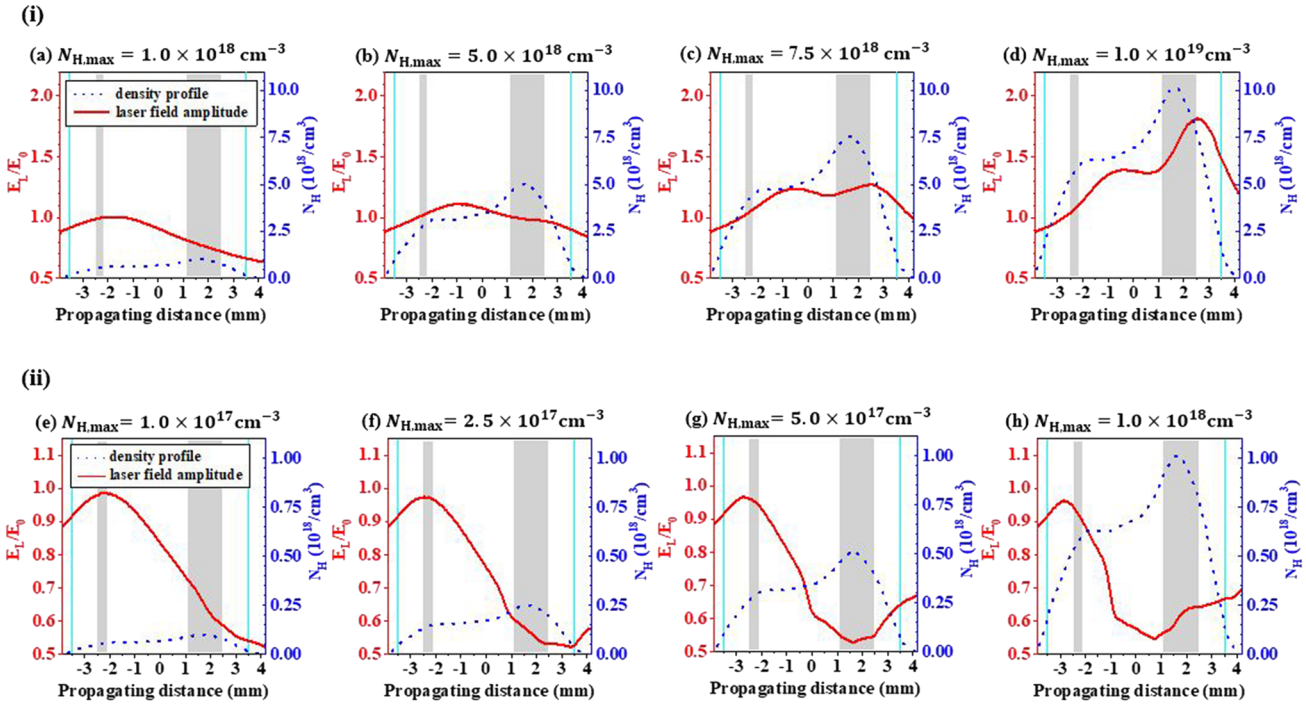

FIG. 9. Propagation of the laser pulse along the longitudinal direction in the capillary, which shows the EPOCH code simulation results for the laser field evolution for different focused laser intensities and hydrogen gas densities. (i) High-intensity laser pulse, $I_0 = 4 \times 10^{17}$ W/cm^2 (fully ionized case). (ii) Low-intensity laser pulse, $I_0 = 2.5 \times 10^{14}$ W/cm^2 (partially ionized case). The blue dotted lines represent the hydrogen gas density profile in the capillary gas cell, and the red solid lines represent the laser field strength. Note that the high-intensity laser pulse of $I_0 = 4 \times 10^{17}$ W/cm^2 is self-focused in a high-density plasma as shown in (c) and (d), but not in a low density plasma [(a) and (b)]. [(e)–(h)] The low-intensity laser pulse of $I_0 = 2.5 \times 10^{14}$ W/cm^2 does not satisfy the self-focusing criterion, and the ionization-induced diffraction effect is dominant.

Figs. 9(e)–9(h). These simulation results show that the ionization-induced diffraction effect becomes more dominant as the plasma density increases.[36]

V. CONCLUSIONS

We successfully developed a capillary gas cell with a longitudinal density gradient. Density tapering was generated by using two feedlines into which hydrogen gas was injected at different pressures. A TW-level femtosecond driving laser pulse was sent to the capillary hole, and a long laser-produced plasma channel was formed by the self-focusing of the driving laser pulse in the plasma. Transverse femtosecond laser interferometry revealed that the capillary gas cell can have a longitudinal plasma density gradient, which may be useful for the suppression of the dephasing problem in laser wakefield acceleration. In future LWFA experiments, we will use the developed capillary gas cell with the high-power Ti:sapphire laser system (after upgrading to 30 TW) in our laboratory.

ACKNOWLEDGMENTS

This work was supported by the National Research Foundation of Korea (Grant No. NRF-2017R1A2B3010765) and GIST (Grant No. GK12200).

DATA AVAILABILITY

The data that support the findings of this study are available from the corresponding author upon reasonable request.

REFERENCES

[1]T. Tajima and J. M. Dawson, "Laser electron accelerator," Phys. Rev. Lett. **43**, 267–270 (1979).
[2]H.-P. Schlenvoigt, K. Haupt, A. Debus, F. Budde, O. Jäckel, S. Pfotenhauer, H. Schwoerer, E. Rohwer, J. G. Gallacher, E. Brunetti, R. P. Shanks, S. M. Wiggins, and D. A. Jaroszynski, "A compact synchrotron radiation source driven by a laser-plasma wakefield accelerator," Nat. Phys. **4**, 130–133 (2008).
[3]N. D. Powers, I. Ghebregziabher, G. Golovin, C. Liu, S. Chen, S. Banerjee, J. Zhang, and D. P. Umstadter, "Quasi-monoenergetic and tunable X-rays from a laser-driven Compton light source," Nat. Photonics **8**, 28–31 (2013).
[4]S. Lee, H. S. Uhm, T. Y. Kang, M. S. Hur, and H. Suk, "Enhanced betatron radiation by a modulating laser pulse in laser wakefield acceleration," Curr. Appl. Phys. **19**, 464–469 (2019).
[5]K. Schmid and L. Veisz, "Supersonic gas jets for laser-plasma experiments," Rev. Sci. Instrum. **83**, 053304 (2012).
[6]A. Döpp, E. Guillaume, C. Thaury, J. Gautier, K. Ta Phuoc, and V. Malka, "3D printing of gas jet nozzles for laser-plasma accelerators," Rev. Sci. Instrum. **87**, 073505 (2016).
[7]S. Lorenz, G. Grittani, E. Chacon-Golcher, C. M. Lazzarini, J. Limpouch, F. Nawaz, M. Nevrkla, L. Vilanova, and T. Levato, "Characterization of supersonic and subsonic gas targets for laser wakefield electron acceleration experiments," Matter Radiat. Extremes **4**, 015401 (2019).
[8]W. P. Leemans, B. Nagler, A. J. Gonsalves, C. Tóth, K. Nakamura, C. G. R. Geddes, E. Esarey, C. B. Schroeder, and S. M. Hooker, "GeV electron beams from a centimetre-scale accelerator," Nat. Phys. **2**, 696–699 (2006).
[9]S. Abuazoum, S. M. Wiggins, B. Ersfeld, K. Hart, G. Vieux, X. Yang, G. H. Welsh, R. C. Issac, M. P. Reijnders, D. R. Jones, and D. A. Jaroszynski, "Linearly tapered discharge capillary waveguides as a medium for a laser plasma wakefield accelerator," Appl. Phys. Lett. **100**, 014106 (2012).
[10]F. Filippi, M. P. Anania, A. Biagioni, E. Brentegani, E. Chiadroni, A. Cianchi, A. Deng, M. Ferrario, R. Pompili, J. Rosenzweig, and A. Zigler, "Tapering of plasma density ramp profiles for adiabatic lens experiments," Nucl. Instrum. Methods Phys. Res., Sect. A **909**, 339–342 (2018).
[11]M. S. Kim, D. G. Jang, T. H. Lee, I. H. Nam, I. W. Lee, and H. Suk, "Characteristics of a tapered capillary plasma waveguide for laser wakefield acceleration," Appl. Phys. Lett. **102**, 204103 (2013).
[12]C. E. Clayton, J. E. Ralph, F. Albert, R. A. Fonseca, S. H. Glenzer, C. Joshi, W. Lu, K. A. Marsh, S. F. Martins, W. B. Mori, A. Pak, F. S. Tsung, B. B. Pollock, J. S. Ross, L. O. Silva, and D. H. Froula, "Self-guided laser wakefield acceleration beyond 1 GeV using ionization-induced injection," Phys. Rev. Lett. **105**, 105003 (2010).
[13]J. Osterhoff, A. Popp, Zs. Major, B. Marx, T. P. Rowlands-Rees, M. Fuchs, M. Geissler, R. Ho¨rlein, B. Hidding, S. Becker, E. A. Peralta, U. Schramm, F. Gru¨ner, D. Habs, F. Krausz, S. M. Hooker, and S. Karsch, "Generation of stable, low-divergence electron beams by laser-wakefield acceleration in a steady-state-flow gas cell," Phys. Rev. Lett. **101**, 085002 (2008).
[14]K. Nakamura, B. Nagler, C. Tóth, C. G. R. Geddes, C. B. Schroeder, E. Esarey, W. P. Leemans, A. J. Gonsalves, and S. M. Hooker, "GeV electron beams from a centimeter-scale channel guided laser wakefield accelerator," Phys. Plasmas **14**, 056708 (2007).
[15]S. Karsch, J. Osterhoff, A. Popp, T. P. Rowlands-Rees, Z. Major, M. Fuchs, B. Marx, R. Hörlein, K. Schmid, L. Veisz, S. Becker, U. Schramm, B. Hidding, G. Pretzler, D. Habs, F. Grüner, F. Krausz, and S. M. Hooker, "GeV-scale electron acceleration in a gas-filled capillary discharge waveguide," New J. Phys. **9**, 415 (2007).
[16]M. Hansson, L. Senje, A. Persson, O. Lundh, C.-G. Wahlström, F. G. Desforges, J. Ju, T. L. Audet, B. Cros, S. D. Dufrénoy, and P. Monot, "Enhanced stability of laser wakefield acceleration using dielectric capillary tubes," Phys. Rev. Spec. Top.–Accel. Beams **17**, 031303 (2014).
[17]S. Kuschel, M. B. Schwab, M. Yeung, D. Hollatz, A. Seidel, W. Ziegler, A. Sävert, M. C. Kaluza, and M. Zepf, "Controlling the self-injection threshold in laser wakefield accelerators," Phys. Rev. Lett. **121**, 154801 (2018).
[18]A. J. Gonsalves, K. Nakamura, C. Benedetti, C. V. Pieronek, S. Steinke, J. H. Bin, S. S. Bulanov, J. van Tilborg, C. G. R. Geddes, C. B. Schroeder, J. Daniels, C. Tóth, L. Obst-Huebl, R. G. W. van den Berg, G. Bagdasarov, N. Bobrova, V. Gasilov, G. Korn, P. Sasorov, W. P. Leemans, and E. Esarey, "Laser-heated capillary discharge plasma waveguides for electron acceleration to 8 GeV," Phys. Plasmas **27**, 053102 (2020).
[19]T. G. Jones, A. Ting, D. Kaganovich, C. I. Moore, and P. Sprangle, "Spatially resolved interferometric measurement of a discharge capillary plasma channel," Phys. Plasmas **10**, 4504 (2003).
[20]A. J. Gonsalves, T. P. Rowlands-Rees, B. H. P. Broks, J. J. A. M. van der Mullen, and S. M. Hooker, "Transverse interferometry of a hydrogen-filled capillary discharge waveguide," Phys. Rev. Lett. **98**, 025002 (2007).
[21]G. Golovin, S. Banerjee, S. Chen, N. Powers, C. Liu, W. Yan, J. Zhang, B. Zhao, and D. Umstadter, "Control and optimization of a staged laser-wakefield accelerator," Nucl. Instrum. Methods Phys. Res., Sect. A **830**, 375–380 (2016).
[22]S. Steinke, J. van Tilborg, C. Benedetti, C. G. R. Geddes, C. B. Schroeder, J. Daniels, K. K. Swanson, A. J. Gonsalves, K. Nakamura, N. H. Matlis, B. H. Shaw, E. Esarey, and W. P. Leemans, "Multistage coupling of independent laser-plasma accelerators," Nature **530**, 190–193 (2016).
[23]M. S. Hur and H. Suk, "Numerical study of 1.1 GeV electron acceleration over a-few-millimeter-long plasma with a tapered density," Phys. Plasmas **18**, 033102 (2011).
[24]W. Rittershofer, C. B. Schroeder, E. Esarey, F. J. Grüner, and W. P. Leemans, "Tapered plasma channels to phase-lock accelerating and focusing forces in laser-plasma accelerators," Phys. Plasmas **17**, 063104 (2010).
[25]Z. Jin, H. Nakamura, N. Pathak, Y. Sakai, A. Zhidkov, K. Sueda, R. Kodama, and T. Hosokai, "Coupling effects in multistage laser wake-field acceleration of electrons," Sci. Rep. **9**, 20045 (2019).
[26]See https://www.ansys.com/ko-kr/academic/free-student-products for information about the Ansys Student version..
[27]See http://www.comatechnology.com/kr/index.php for information about Coma Technology Co..

[28]I. Nam, M. Kim, T. H. Lee, S. W. Lee, and H. Suk, "Highly-efficient 20 TW Ti:sapphire laser system using optimized diverging beams for laser wakefield acceleration experiments," Curr. Appl. Phys. **15**, 468–472 (2015).
[29]S. Augst, D. D. Meyerhofer, D. Strickland, and S. L. Chint, "Laser ionization of noble gases by Coulomb-barrier suppression," J. Opt. Soc. Am. B **8**, 858–867 (1991).
[30]F. Keilmann, "An infrared Schlieren interferometer for measuring electron density profiles," Plasma Phys. **14**, 111–122 (1972).
[31]C. M. Vest, "Interferometry of strongly refracting axisymmetric phase objects," Appl. Opt. **14**, 1601–1606 (1975).
[32]E. Hecht, *Optics* (Addison-Wesley, Boston, 2001), Chap. 7.
[33]E. Esarey, C. B. Schroeder, and W. P. Leemans, "Physics of laser-driven plasma-based electron accelerators," Rev. Mod. Phys. **81**, 1229–1285 (2009).
[34]J. Faure, V. Malka, J.-R. Marquès, P.-G. David, F. Amiranoff, K. Ta Phuoc, and A. Rousse, "Effects of pulse duration on self-focusing of ultra-short lasers in underdense plasmas," Phys. Plasmas **9**, 756–759 (2002).
[35]T. D. Arber, K. Bennett, C. S. Brady, A. Lawrence-Douglas, M. G. Ramsay, N. J. Sircombe, P. Gillies, R. G. Evans, H. Schmitz, A. R. Bell, and C. P. Ridgers, "Contemporary particle-in-cell approach to laser-plasma modelling," Plasma Phys. Controlled Fusion **57**, 113001 (2015).
[36]P. Gibbon, *Short Pulse Laser Interactions with Matter* (World Scientific, Singapore, 2005), Chap. 2, pp. 24–27.